Electron-impact scattering by arsine

Jaspreet Kaur, Biplab Goswami, Dhanoj Gupta, and Bobby Antony*
Department of Applied Physics, Indian School of Mines, Dhanbad 826004, Jharkhand, India
(Received 14 March 2014; published 31 July 2014)

We present elastic cross sections for electron interactions with arsine (AsH_3) in gas phase over an extensive energy range from 0.5 to 5000 eV by combining two computational methods. The *ab initio* *R*-matrix method is employed for low-energy computations up to 15 eV and the intermediate to high-energy calculations were performed using the spherical complex optical potential (SCOP) method. The elastic cross section computed through the *R* matrix and SCOP formalism shows consistency at crossover energy (11–12 eV) and gives reasonable accord with the available data. Besides elastic cross sections, the differential cross section at low and intermediate incident electron energies is reported. The electronic excitation cross section is also reported at low energies. Shape resonance is observed at around 2.4 eV due to the formation of a transient negative ion state.

DOI: 10.1103/PhysRevA.90.012711 PACS number(s): 34.80.Bm, 34.80.Ht, 34.50.Gb

I. INTRODUCTION

Arsine (AsH_3) is a highly toxic gas. It is one of the simplest compounds of arsenic and is used for the synthesis of organoarsenic compounds [1]. Despite its toxicity, it is extensively used in the semiconductor industry for epitaxial growth of gallium arsenide (GaAs) and GaInAsN. For microelectronic applications, arsine is provided via a subatmospheric gas source. Heteroepitaxial films of GaInAs have been grown on GaAs substrates by the reaction of triethylindium and trimethylgallium with arsine gas [2]. It is also used to make the semiconductor GaAs by metal organic chemical vapor deposition [3]. Besides, AsH_3 gas is frequently used as an *n*-type dopant for Ge [4–6] and SiGe [7] in metal organic vapor phase epitaxy and chemical vapor deposition technique in microelectronic devices. In fact, plasma etching, plasma deposition, and several other plasma-based processes are the foundation of the microelectronics industry. Therefore electron interaction data for arsine are required for the study and effective use in plasma-assisted thin-film deposition, plasma etching, and for surface treatment and cleaning.

Recently, arsine has been detected in the atmosphere of Saturn [8]. Low-energy electronic excitation of molecular targets is an important energy-loss mechanism in molecular gases. Therefore, the scattering of slow electrons by molecules and the respective cross sections are of crucial importance in the modeling of planetary atmosphere. The relevant cross sections are also required in determining the electron velocity distribution in gaseous discharge, electron drift experiments [9], and in the description of cold plasma [10–12] and laser development [13].

Due to its lethality, to perform an electron scattering experiment with this molecule is quite difficult. Consequently, more work is required on the collision cross-section measurement for e-AsH_3. Winstead *et al.* [14] computed integral, differential, and momentum transfer elastic cross sections for e-AsH_3 scattering using the all-electron Schwinger multichannel method (SMCAE) [15]. Bettega *et al.* [11] have reported theoretical electron-impact elastic cross sections in the energy range 10–30 eV by employing the Schwinger multichannel method with psuedopotentials (SMCPP) [16] approximation. Later, Bettega and Lima [17] calculated the integral cross section for the 0.5–8 eV energy regime. It is clear that cross-section data reported for this molecule are quite fragmentary and have been restricted to a limited energy range.

In this article, the elastic cross section is reported over a wide energy range (0.5–5000 eV) by utilizing two computational methods adjoining each other at about the ionization potential of the target. For the low incident electron energies, calculations were performed using the *R*-matrix [18] method through the QUANTEMOL-N software package [19]. For energies above the ionization threshold, spherical complex optical potential (SCOP) [20–23] formalism is employed. Our focus is also on localizing the resonance which appears as a sharp feature in the cross-section curve. Resonance occurs due to the formation of a transient negative ion state by temporary trapping of the incident electron inside the molecule at well defined energy. A resonance may lead to the dissociation of the molecule into neutral and anionic fragments or leave the target molecule in the vibrationally excited state after the ejection of impinging electron. In addition to this, we report the excitation and differential cross sections for e-AsH_3 system for low electron-impact energies using the close-coupling *R*-matrix method. The differential cross section (DCS) is also calculated at intermediate energies using SCOP formalism.

The subsequent sections will give an account of the theoretical methodologies applied for the computations, results, and discussion, and finally the conclusions.

II. THEORETICAL METHODOLOGY

In this section a brief idea about our theoretical approaches applied for evaluating various cross sections are presented. The low-energy *ab initio* calculations below 15 eV were carried out using the *R*-matrix method through the QUANTEMOL-N software package. For incident electron energies above the ionization threshold of the target (up to 5 keV), SCOP formalism is employed. The accuracy of cross sections calculated through the *R*-matrix method depends primarily on the correct representation of the target. This is verified by comparing the target parameters obtained using the best available wave function, so, it is mandatory to discuss the target model employed for the low-energy calculation before

*bka.ism@gmail.com

 ©2014 American Physical Society

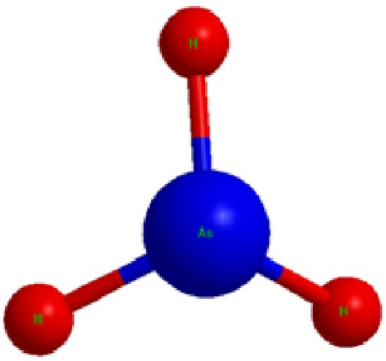

FIG. 1. (Color online) Structure of arsine.

we proceed to explain the theoretical methodologies used to calculate the cross sections.

A. Target representation

Arsine has ammonialike trigonal pyramidal geometry, but with a smaller bond angle (Fig. 1). Although the natural symmetry of AsH_3 belongs to the C_{3v} point group; we have considered it in the C_s point group with the cc-pVDZ basis set while defining its wave function due to the restriction of the R-matrix code. The C_s point group is considered as it is the subgroup of C_{3v}. A_1, A_2, and E irreducible representations of C_{3v} correlate to A', A'' and $A'+A''$ of C_s, respectively. The ground state Hartree-Fock electronic configuration is $1a'^2$, $2a'^2$, $1a''^2$, $3a''^2$, $4a'^2$, $5a'^2$, $2a''^2$, $6a'^2$, $7a'^2$, $8a'^2$, $3a''^2$, $4a''^2$, $9a'^2$, $10a'^2$, $11a'^2$, $12a'^2$, $13a'^2$, and $14a'^2$. Among these, 18 core electrons of the target are frozen and do not take part in the calculations. The remaining 18 electrons are kept in the active space. The orbitals corresponding to frozen electrons are $1a'$, $2a'$, $3a'$, $4a'$, $5a'$, $6a'$, $7a'$, $1a''$, and $2a''$ whereas the active space involves the following orbitals: $8a'$, $9a'$, $10a'$, $11a'$, $12a'$, $13a'$, $14a'$, $15a'$, $3a''$, $4a''$, $5a''$, and $6a''$. The idea here is to keep an optimum number of electrons in the active region for reliable scattering calculations. A total number of 7954 configuration state functions (CSFs) are generated for the 12 target states for the ground state and 155 channels are incorporated into the scattering calculations.

A correct target representation yields reliable target parameters in the inner region, which ensures good cross-section data in the outer region. The target parameters obtained from the inner region calculations employing the present model are shown in Table I. There is good agreement of calculated parameters with the available comparisons.

TABLE I. Target properties.

Properties of AsH_3	Present	Experimental	Theoretical
Ground-state energy (hartree)	–2235.906	–	–2235.826 [24]
First excitation energy (eV)	6.339	–	–
Rotational constant (cm^{-1})	3.8015	3.75154 [25]	–
Dipole moment (D)	0.2863	0.20 [26]	0.2638 [17]

B. Low-energy formalism

The *ab initio* R-matrix method is one of the widely used approaches for electron scattering calculations besides other close-coupling formalisms such as the complex Kohn variational method (CKVM) [27] and the Schwinger multichannel (SMC) method [15]. All these methods are well established and have underlying similarities among them. The basic idea in all of the three variational methods is designing the wave function to solve the Schrödinger equation for the scattering system of $N+1$ electrons in a fixed nuclei approximation. In the SMC method, the Schrödinger equation is replaced by the Lippmann-Schwinger equation. This equation involves the use of the Green's function to perform the computations. The advantage of the SMC method is that all matrix elements, including those of the Green's function, involve the electron-molecule interaction which vanishes at large radial distances. In contrast, in the CKVM and R-matrix methods no boundary conditions have to be satisfied by a trial wave function, which is taken care of by the Green's function in the SMC method. On the other hand, the CKVM method is a more computationally stable approach as it avoids the computation of the Green's function matrix elements. Only matrix elements of the Hamiltonian appear in the calculations. Exchange matrix elements involving continuum functions are eliminated rigorously from these calculations. The asymptotic behavior of the trial wave function must be specified in this method. In general all three methods are found to be quite successful in calculating the cross section and predicting the resonances located at low energies.

In the present work we have employed the R-matrix method, which is an accurate procedure for low-energy electron scattering studies. The method works on the principle of division of configuration space into two concentric spherical regions, namely, the inner and outer regions. The inner region radius is chosen such that all the short-range interactions are contained within it. The target wave function and corresponding charge density are assumed to be completely included in this sphere and the electron-target interaction is represented through exchange and correlation potentials. Invariably, the physics in this region is sophisticated and the R-matrix method is realized numerically by the adaptation of quantum chemistry codes. However, the solution is energy independent and hence required to be solved only once. On the other hand, the outer region is solved with simplified equations. Here, long-range multipolar interactions of the scattering electrons with different target states are considered using a single center close-coupling approximation. At the interface, the energy-independent solutions from the inner region are used to construct an energy-dependent R matrix. The inner region radius is taken as 10 a_o whereas the outer region spans to 100 a_o.

The inner region wave function is constructed using the close-coupling approximation. Within this framework the inner region wave function is written as

$$\psi_k^{N+1} = A \sum_I \psi_I^N(x_1, \ldots, x_N) \sum_j \xi_j(x_{N+1}) a_{Ijk} + \sum_m \chi_m(x_1, \ldots, x_{N+1}) b_{mk}, \quad (1)$$

where A is the antisymmetrization operator and a_{Ijk} and b_{mk} are variational coefficients determined by the diagonalization of the Hamiltonian matrix. The space-spin coordinates of the electron are represented by $x_N(r_N,\sigma_N)$. The first summation takes into account the close coupling of all the target-plus-continuum states and has a single Hartree-Fock target state in the static exchange calculation. The second summation involves configurations χ_m and has zero amplitude on the R-matrix boundary. Here, all electrons are placed in the associated target molecular orbitals and they permit relaxation of the orthogonalization between the continuum and target orbitals and include target polarization effects. Then, the Hartree-Fock self-consistent method gives a complete description of the virtual and occupied orbitals using Gaussian-type molecular orbitals and continuum orbitals of Faure *et al.* [28]. Here we have included orbitals up to g, i.e., $l = 4$. The molecules with dipole moment have a cross section that becomes very large at low scattering energies and angles and therefore corrections are made in the calculations. For this the contributions due to higher partial waves (i.e., $l > 4$) are included by applying a Born correction at all energies.

In the fixed nuclei (FN) approximation, the elastic cross section of molecules with permanent dipole moment usually diverges in a forward scattering direction. This divergence can also be attributed to the long-range nature of dipole interaction in an electron-molecule collision. Since the electron-molecule interactions decay slowly with the distance between them, the partial-wave expansion often converges slowly. To overcome these obstacles and accelerate the convergence of higher partial waves, the Born closure method has been proposed. This closure method implements the Born correction using two approaches. The first approach is to use a closure formula at the partial cross-section level and in the second approach correction is implemented at the T-matrix level. The expressions for the partial as well as full Born cross sections are required for correction at the cross-section level. In the closure approximation, there is an evaluation of partial cross section σ_l^R and σ_l^B in the R matrix and Born approximation, respectively, for all the partial values up to the g wave. Then, the integrated Born cross section, σ^B is added as follows to obtain the Born corrected cross section:

$$\sigma = \sum_{l=0}^{4} \left(\sigma_l^R - \sigma_l^B\right) + \sigma^B. \tag{2}$$

After obtaining the R matrix at the boundary, the next objective is to obtain the final, energy-dependent solutions of the scattering problem. However, there are two major obstacles in these calculations. The first problem is due to the lower symmetry of the target and much stronger long-range potentials. The second is due to several degenerate channels associated with each target state. The common practice to address the outer region problem involves two stages. First the R matrix is propagated from the inner region boundary ($r = 10\ a_o$) to the outer region boundary. Here the non-Coulomb potential can be neglected beyond the asymptotic region. To obtain the asymptotic solution, the expansion method given by Gailitis [29] is employed. Thus the outer region solution for the wave function is obtained in the form of K matrices In fact, all the scattering observables can be extracted from the K matrices. Using K matrices the eigenphase sum can be obtained from its eigenvalues as

$$\delta = \sum_i \arctan(K_{ii}). \tag{3}$$

The resonance parameters, viz., position and width, are extracted from the eigenphase sum using the resonance detection program RESON [30], which matches the eigenphase sum to a Breit-Wigner form [31]. However, to determine the scattering cross section we should evaluate the T matrices, which can be derived from the K matrices using the expression

$$T = \frac{2iK}{1 - iK}. \tag{4}$$

By employing these T matrices the total cross sections are evaluated using standard relations. The differential cross-section (DCS) data at low energies are also calculated using the K matrices through the POLYDCS program of Sanna and Gianturco [32].

C. High-energy formalism

For incident electron energies above the ionization threshold of the target molecule, the calculations have been carried out using the well established SCOP formalism. The e-AsH_3 scattering dynamics is represented in terms of the interaction potential called the spherical complex optical potential [20–23]. This complex optical potential comprises real and imaginary parts, represented as

$$V_{\text{opt}}(r,Ei) = V_{\text{st}}(r,Ei) + V_{\text{ex}}(r,Ei) + Vp(r,Ei) + iV_{\text{abs}}(r,Ei), \tag{5}$$

wherein the real potentials, V_{st}, V_{ex}, V_p, and V_{abs}, are the static, exchange, polarization, and absorption potentials, respectively. V_{st} is the electrostatic Coulomb interaction of the incoming projectile (electron) with the target, V_{ex} fulfills the antisymmetrization criteria on the wave function, and V_p results from the correlation between the projectile and the target due to the induced dipole moments in the field of the incoming electron. The V_{abs} appearing in the expression accounts for the loss of scattered flux to the outgoing channels. Altogether, these potentials describe an electron-target scattering system and depend primarily on the radial charge distribution, dipole polarizability, and the ionization potential of the target. The molecule radial charge density is determined from the atomic charge densities formulated through the parametrized Hartree-Fock (HF) wave function of Cox and Bonham [33]. In the present case a lighter hydrogen atom is attached with a relatively heavier arsenic atom. The atomic hydrogen charge density is expanded from the center of the arsenic atom using the Bessel function expansion method given by Gradashteyn and Ryzhik [34] and the sum of the charge density of the arsenic atom and the expanded charge densities of hydrogen atoms gives the molecular charge distribution. For the static potential, the HF parameters given by Cox and Bonham [33] were employed. Hara's free electron model [35] and the correlation model of Zhang *et al.* [36] are used for the exchange and polarization potentials, respectively. In the model of Zhang *et al.* [36] various multipole nonadiabatic corrections are incorporated in the intermediate region to give

the appropriate asymptotic form. The imaginary part of the interaction potential is modeled from the potential introduced by Staszewska *et al.* [37] given by

$$V_{\rm abs}(r,E_i) = -\rho(r)\sqrt{\frac{T_{\rm loc}}{2}}\left(\frac{8\pi}{10k_F^3E_i}\right)$$
$$\theta\left(p^2-k_F^2-2\Delta\right)(A_1+A_2+A_3), \quad (6)$$

where the local kinetic energy, $T_{\rm loc} = E_i - (V_{\rm st} + V_{\rm ex} + V_p)$, and the parameters A_1, A_2, A_3 are defined as

$$A_1 = \frac{5k_f^3}{2\Delta};\ A_2 = -\frac{k_f^3\left(5p^2-3k_f^3\right)}{\left(p^2-k_f^2\right)^2};$$

$$A_3 = 2\theta\left(2k_f^2+2\Delta-p^2\right)\frac{\left(2k_f^2+2\Delta-p^2\right)^{5/2}}{\left(p^2-k_f^2\right)^2}.$$

$p^2 = 2E_i$, $k_F = [3\pi^2\rho(r)]^{1/3}$ is the Fermi wave vector and Δ is the energy parameter. The energy parameter prevents ionization or excitation of the target below the ionization threshold and consequently leads to $V_{\rm abs} = 0$ for $\Delta \le I$. Further, $\theta(x)$ is the Heaviside unit step function where $x = p^2 - k_F^2 - 2\Delta$. Now, these model potentials are incorporated into the Schrödinger equation which is solved by partial-wave analysis implementing the Numerov method for the present scattering system. The solutions are obtained in terms of complex phase shifts (δ_l) that have the signature of electron-target interaction for each partial wave. The convergence of the partial waves was checked for obtaining reliable results. Thus for higher energies a large number of phase shifts were required as compared to low incident electron energies. The inelasticity or the absorption factor is then calculated from the phase shifts for each partial wave and is given by

$$\eta_l = \exp(-2{\rm Im}\delta_l). \quad (7)$$

The elastic cross sections [38] are computed from the absorption factor by the expressions

$$Q_{\rm el}(E_i) = \frac{\pi}{k^2}\sum_{l=0}^{\infty}(2l+1)|\eta_l\exp(2i{\rm Re}\delta_l) - 1|^2. \quad (8)$$

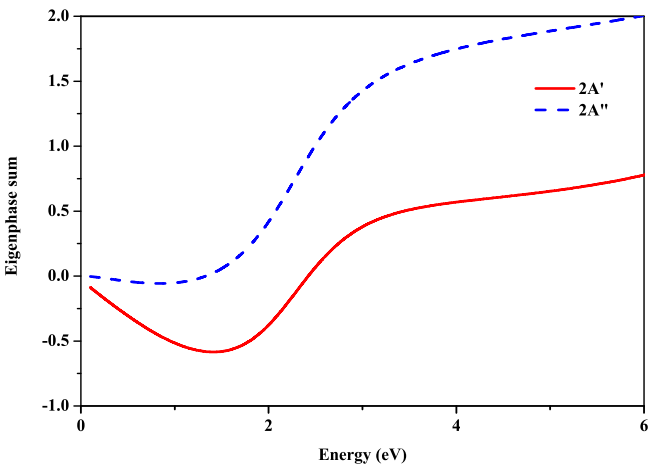

FIG. 2. (Color online) Doublet eigenphase sum for arsine.

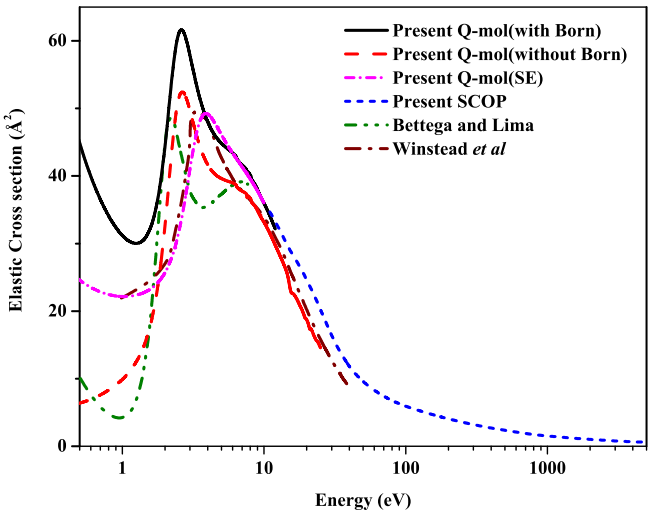

FIG. 3. (Color online) Present elastic cross section for e-AsH_3 collisions. Solid line: present (with Born correction); dashed line: present (without Born correction); short dash dot: present Q-mol (SE); short-dashed line: present SCOP; dash-dot-dot line: Bettega and Lima (SMCPP) [17]; dash-dot-dash line: Winstead *et al.* (SMCAE) [14].

III. RESULTS AND DISCUSSION

The results obtained in the present calculation are discussed in this section. In Fig. 2, we have plotted the eigenphase sum which is quite important to identify resonance structures at low energies. The elastic cross section over an extensive range of energy from 0.5 to 5000 eV is plotted in Fig. 3. As discussed earlier the two methodologies are applied for evaluating data over such a wide energy range. There is an excellent matching at the overlapping energy (∼11–12 eV), which justifies the use of two formalisms at two energy regimes. The excitation and differential cross sections at low electron energies calculated by the R-matrix method are presented in Figs. 4 and 5, respectively. Differential cross sections are also calculated using SCOP formalism for intermediate energies as shown in Fig. 6.

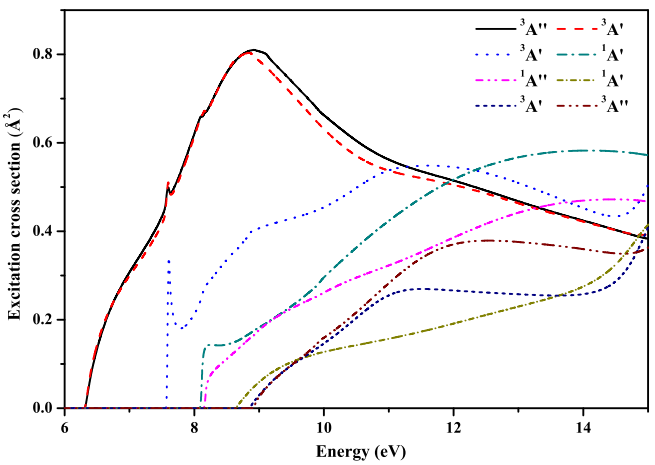

FIG. 4. (Color online) Electronic excitation cross section for e-AsH_3 scattering to different singlet and triplet states.

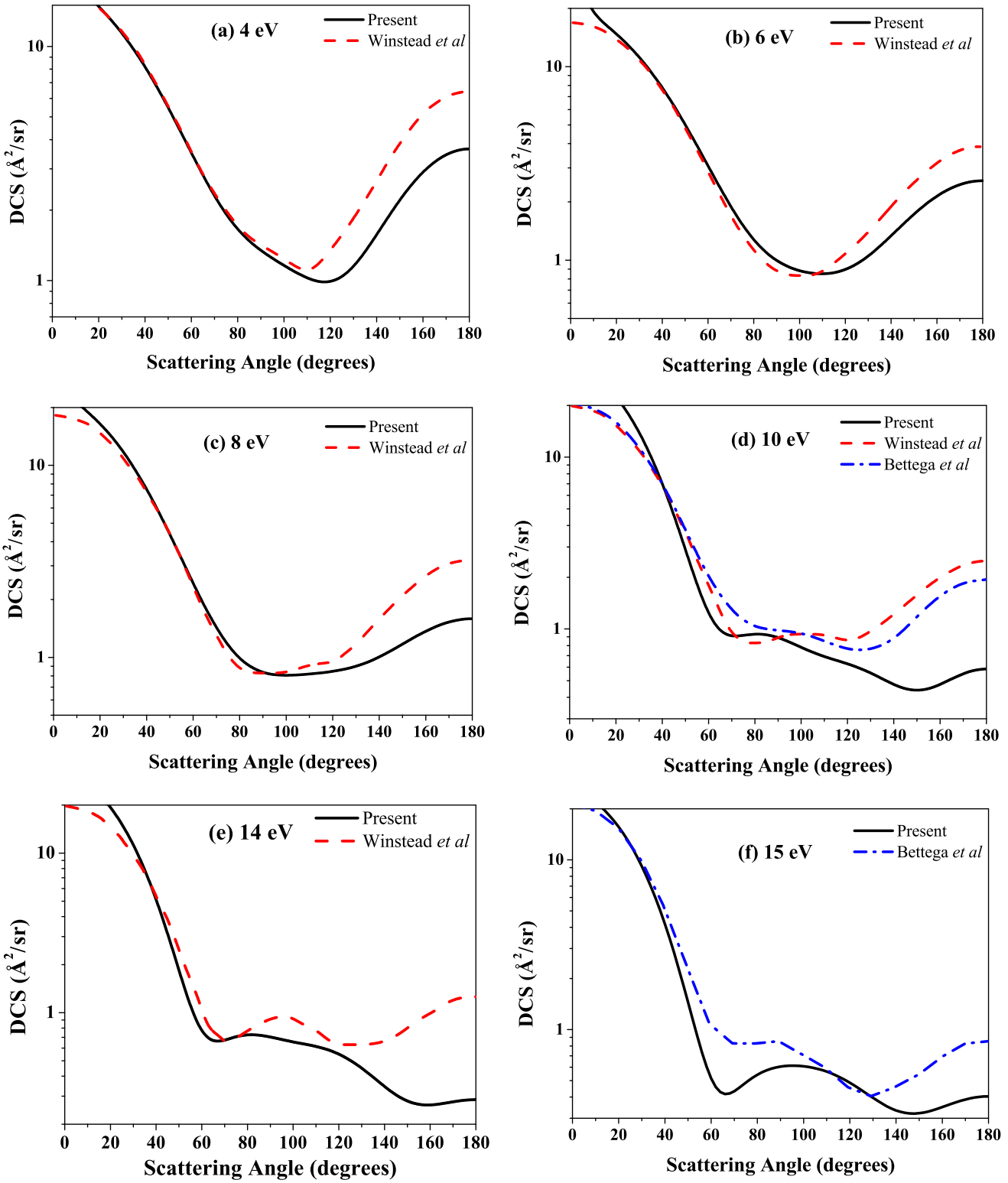

FIG. 5. (Color online) Elastic DCS for e-AsH_3 scattering. Solid line; present; dashed line: Winstead *et al.* (SMCAE) [14]; dash-dot line: Bettega *et al.* (SMCPP) [11].

Figure 2 illustrates the energy dependence of the eigenphase sum for the e-AsH_3 system. In the low-energy regime, the study of the eigenphase sum finds significance as it reflects the position of the resonance structure in this energy range. In Fig. 2 the eigenphase sum for different symmetries of the C_s point group involved in the scattering event are depicted. The present calculation identifies a shape resonance at around 2.4 eV corresponding to the E symmetry of the C_{3v} group with a resonance width of 1.4 eV. There is a lowering of the symmetry from C_{3v} to C_s which causes the twofold degenerate

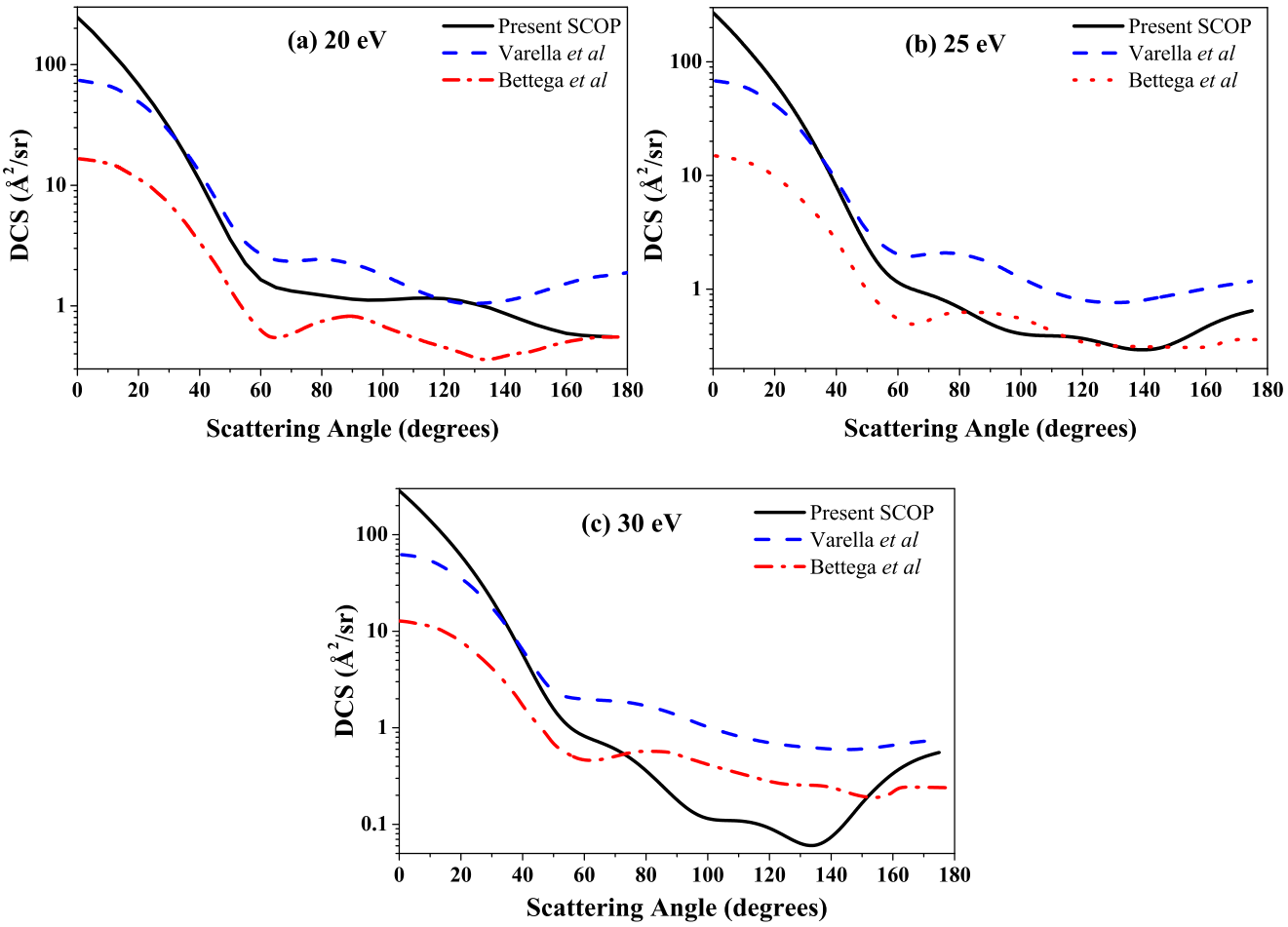

FIG. 6. (Color online) Elastic DCS for e-AsH_3 scattering. Solid line: present; dashed line: Varella *et al.* (SMCPP) [39]; dash-dot line: Bettega *et al.* (SMCPP) [11].

E symmetry to split into the degenerate A' and A'' components in the C_s point group. Being degenerate symmetries, the position of resonance in A' and A'' should be located at the same energy. However, a deviation of 0.13 eV is observed in our calculation due to the unbalanced treatment of polarization between the A' and A'' symmetries of the C_s point group.

Figure 3 shows the present elastic cross section for the e-AsH_3 scattering in static exchange (SE) and close-coupling approximation along with the theoretical results of Winstead *et al.* [14] and Bettega and Lima [17]. Qualitatively, the present elastic cross sections show fair agreement in terms of peak position at low energies with Bettega and Lima [17]. Also, the nature of the cross section is similar to Bettega and Lima [17] and a noticeable dip is also observed at around 4 eV. The cross-section curve shows a sharp structure at around 2.4 eV due to the twofold-degenerate E symmetry of the C_{3v} group, which splits into the A' and A'' symmetries of the C_s group which corresponds to the characteristic resonance observed as discussed earlier. Resonance phenomena signify the temporary trapping of electrons within the unoccupied molecular orbitals or can excite any of the occupied molecular orbitals.

The present cross section without Born correction is in good accord with the previously reported theoretical values. The present elastic cross section is plotted up to 5000 eV and shows slightly higher but close agreement with Bettega and Lima [17] for the compared energy range. The cross section with Born correction includes the effect of higher partial waves and also the target dipole moments. So, the cross section obtained with Born correction is higher than those without Born correction. Present methodology includes the polarization effect which usually gives better results than calculations having static exchange in their formalism. The peak positions of the cross section reported by Winstead *et al.* [14] are a little higher than the present cross-section values. They have reported resonance for the E symmetry at 3.5 eV. This may be due to the neglect of target polarization effects and scattering due to other open channels. However, the nature and magnitude of the present cross section in the SE approximation agree fairly well with those of Winstead *et al.* [14]. The resonance structure identified in the present SE approximation is at 3.25 eV which is in close proximity to the resonance position predicted by Winstead *et al.* [14] using the same approximation. The cross section beyond 10 eV decreases monotonically and shows a transition of cross-section data calculated using two methods at crossover energy (11–12 eV).

Figure 4 shows the excitation cross section for electron-arsine scattering to various singlet and triplet excited states (A' and A'') from the ground state due to the excitation of the target from occupied (hole) orbitals to a set of allowed unoccupied (particle) orbitals. From the curve we can infer

TABLE II. Excitation threshold energies.

States	Vertical excitation energy (eV)
$^1A'$	0.00
$^3A'$	6.33
$^3A''$	6.33
$^3A'$	7.59
$^1A'$	8.10
$^1A''$	8.16
$^1A'$	8.65
$^3A'$	8.87
$^3A''$	8.92
$^3A'$	9.11
$^3A''$	9.87
$^1A''$	9.95

that the thresholds of excitation for triplet and singlet states are 6.33 and 8.10 eV, respectively. The threshold for the $^3A''$ and $^3A'$ excitation cross section is exactly the same. It is evident from the figure that the triplet excitations contribute more than other excitations. Moreover, the cross sections for triplet states are larger than the corresponding singlet states due to their larger spin multiplicity and lower thresholds. The threshold of excitation and the excitation cross-section values for the AsH_3 molecule is reported for the first time. Table II reports the calculated vertical excitation energies for different singlet and triplet excitations.

The DCS is calculated for energies from 0.5 to 15 eV at the scattering angles 0°–180° employing R-matrix codes. However, for brevity it is plotted only for energies for which comparisons are available. Figures 5(a)–5(f) show the DCSs for energies 4, 6, 8, 10, 14, and 15 eV. The DCS is compared with the results of Bettega *et al.* [11] and Winstead *et al.* [14]. The present results show very good agreement with other theoretical results presented here. The large cross sections in the forward direction are due to the dipolar nature of the target. The oscillatory behavior in the DCS curve may be due to the coupling of higher partial waves of the heavier arsenic atom in the electron collision process. There is excellent accord at forward scattering angles, but a slight deviation occurs at backward scattering angles. Our results are a little lower than previous results [11,14] at backward scattering angles as also observed for the disilane molecule [23]. This may be attributed to the constraints in the R-matrix method due to which some virtual orbitals are localized within the R-matrix sphere. So, our close-coupling calculations incorporate the polarization effects at short range where they are strongest. When the electron is outside the R-matrix sphere, long-range polarization comes into play. However, there is an intermediate region where our calculations cannot properly model the polarization effects. Thus, the systematic inclusion of polarization at short, intermediate, and long range could alter the calculated large-angle behavior. However, such calculations are computationally expensive and are yet to be implemented for many targets. We have also computed DCS using SCOP formalism for 20, 25, and 30 eV as shown in Figs. 6(a)–6(c). The computed DCS is compared with the available results of Varella *et al.* [39] and Bettega *et al.* [11]. They have computed elastic DCS using the SMCPP method in the SE approximation. The agreement of the present results is fair enough as compared to previous results [11,39]. In fact all the previous results along with the present one show some deviation from each other. An experimental investigation for these energies would be useful to quantify the results.

IV. CONCLUSION

A detailed study of electron collision with arsine molecule is undertaken in this work. We have presented the results for various cross sections, viz., elastic, excitation, and differential cross sections for the e-AsH_3 scattering. The elastic cross section is reported over a wide energy domain from 0.5 to 5000 eV using two theoretical formalisms: R matrix and SCOP. The target properties obtained in the present calculation are found to compare very nicely with existing values. We have identified a prominent shape resonance at around 2.4 eV corresponding to the E symmetry of the C_{3v} point group which splits into the two components A' and A'' symmetries of the C_s group. Resonance in the cross-section curve is a manifestation of the formation of a negative molecular ion for a finite time that decays into the energetically open channels. The elastic cross section presented here gives satisfactory agreement with previous theoretical values wherever available. We have not found any comparisons for elastic cross sections above 40 eV for e-AsH_3 scattering. The DCS reported by us also shows good comparison with the available values of Winstead *et al.* [14], Bettega *et al.* [11], and Varella *et al.* [39] at selected energies. The differences of cross section between present and previous theories may be due to the incorporation of polarization effects besides static and exchange in our calculation. It has been already understood that the model which includes polarization effects such as static exchange plus polarization (SEP) or close coupling gives better results compared to SE results, especially at low incident energies. The present DCS shows good agreement with the previous results, in terms of shape and magnitude at forward angles. However, our results seem to underestimate them towards the backward scattering region.

We hope that the dearth of data on the e-AsH_3 scattering system compels experimental and further theoretical investigations, considering its applications along with its hazardous effects.

ACKNOWLEDGMENTS

B.A. is pleased to acknowledge the support of this research by the Department of Science and Technology (DST), New Delhi, through Grant No. SR/S2/LOP-11/2013.

[1] A. F. Holleman and E. Wiberg, *Inorganic Chemistry* (Academic Press, San Diego, 2001).

[2] B. J. Baliga and S. K. Ghandhi, J. Electrochem. Soc. **122**, 683 (1975).

[3] *Chemistry of Electronic Materials*, edited by A. R. Barron (Rice University, Houston, 2011).
[4] M. Takenaka, K. Morii, M. Sugiyama, Y. Nakano, and S. Takagi, Jpn. J. Appl. Phys. **50**, 010105 (2011).
[5] W. E. McMahon and J. M. Olson, J. Cryst. Growth **225**, 410 (2001).
[6] S. Gan, L. Li, M. J. Begarney, D. Law, B.-K. Han, and R. F. Hicks, J. Appl. Phys. **85**, 2004 (1999).
[7] E. Suvar, J. Christensen, A. Kuznetsov, and H. H. Radamson, Mater. Sci. Eng., B **102**, 53 (2003).
[8] B. Bezard, P. Drossart, E. Lellouch, G. Tarrago, and J. P. Maillard, Astrophys. J. **346**, 509 (1989).
[9] K. Takayanagi and K. Itikawa, Adv. At. Mol. Phys. **6**, 105 (1970).
[10] A. Garscadden, Z. Phys. D **24**, 97 (1992); all articles in this issue are devoted to relevant phenomena that take place in cold plasma.
[11] M. H. F. Bettega, M. A. P. Lima, and L. G. Ferreira, J. Chem. Phys. **105**, 1029 (1996).
[12] J. Yuan and Z. Zhang, Z. Phys. D **28**, 207 (1993).
[13] D. W. Norcross and L. A. Collins, Adv. At. Mol. Phys. **18**, 341 (1982).
[14] C. Winstead, Q. Sun, V. McKoy, J. L. d. S. Lino, and M. A. P. Lima, Z. Phys. D **24**, 141 (1992).
[15] K. Takatsuka and V. McKoy, Phys. Rev. A **24**, 2473 (1981); **30**, 1734 (1984).
[16] M. H. F. Bettega, L. G. Ferreira, and M. A. P. Lima, Phys. Rev. A **47**, 1111 (1993).
[17] M. H. F. Bettega and M. A. P. Lima, J. Phys. B **37**, 3859 (2004).
[18] J. Tennyson, Phys. Rep. **491**, 29 (2010).
[19] J. Tennyson, D. B. Brown, J. J. Munro, I. Rozum, H. N. Varambhia, and N. Vinci, J. Phys.: Conf. Ser. **86**, 012001 (2007).
[20] A. Jain and K. L. Baluja, Phys. Rev. A. **45**, 202 (1992).
[21] M. Vinodkumar, A. Barot, and B. K. Antony, J. Chem. Phys. **136**, 184308 (2012).
[22] M. Vinodkumar, H. Bhutadia, B. K. Antony, and N. J. Mason, Phys. Rev. A **84**, 052701 (2011).
[23] D. Gupta, R. Naghma, B. Goswami, and B. K. Antony, RSC Adv. **4**, 9197 (2014).
[24] CCCBDB at http://cccbdb.nist.gov.
[25] G. S. Blevins, A. W. Jache, and W. Gordy, Phys. Rev. **97**, 684 (1955).
[26] R. D. Nelson, Jr., D. R. Lide, and A. A. Maryott, NSRDS-NBS-10 (1967), See website: http://www.nist.gov/data/nsrds/NSRDS-NBS-10.pdf.
[27] T. N. Rescigno and B. I. Schneider, Phys. Rev. A **45**, 2894 (1992); T. N. Rescigno, B. H. Lengsfield, C. W. McCurdy, and S. D. Parker, *ibid.* **45**, 7800 (1992).
[28] A. Faure, D. Gorfinkiel, L. A. Morgan, and J. Tennyson, Comput. Phys. Commun. **144**, 224 (2002).
[29] M. Gailitis, J. Phys. B **9**, 843 (1976).
[30] J. Tennyson and C. J. Noble, Comput. Phys. Commun. **33**, 421 (1984)
[31] G. Breit and E. Wigner, Phys. Rev. **49**, 519 (1936).
[32] N. Sanna and F. A. Gianturco, Comput. Phys. Commun. **114**, 142 (1998).
[33] H. L. Cox and R. A. Bonham, J. Chem. Phys. **47**, 2599 (1967).
[34] Gradashteyn and I. M. Ryzhik, *Tables of Integrals, Series and Products* (Associated Press, New York, 1980).
[35] S. Hara, J. Phys. Soc. Jpn. **22**, 710 (1967).
[36] X. Zhang, J. Sun, and Y. Liu, J. Phys. B **25**, 1893 (1992).
[37] G. Staszewska, D. W. Schwenke, D. Thirumalai, and D. G. Truhlar, Phys. Rev. A **28**, 2740 (1983).
[38] C. J. Joachain, *Quantum Collision Theory* (North-Holland, Amsterdam, 1983).
[39] M. T. N. Varella, M. H. F. Bettega, A. J. R. Silva, and M. A. P. Lima, J. Chem. Phys. **110**, 2452 (1999).